JOURNAL OF MATERIALS SCIENCE 33 (1998) 1851–1856

Influence of the silica matrix on the formation of α-alumina in a mullite–alumina composite from a diphasic precursor

MINGHUA ZHOU, J. M. F. FERREIRA, A. T. FONSECA
Department of Ceramic and Glass Engineering, University of Aveiro, 3810 Aveiro, Portugal

In mullite–alumina composite precursors, interaction between the silica matrix and the fine γ-alumina texture strongly influences the precursor phase transformation, the nucleation and the crystal geometry both of the mullite and of the α-alumina. The mullite–alumina composite precursor calcined at 1000 °C has a layered structure probably derived from the layered texture of the γ-alumina. The phase transition of this layered texture is retarded by the presence of the silica matrix and a metastable mullite phase is formed before nucleation of α-alumina. By leaching away the silica matrix, the remaining layered texture is readily transformed into very fine, thin α-alumina platelets by calcination at 1000 °C. This seems to be one reason for the appearance of elongated mullite grains in a pure mullite matrix and the platelet shaped α-alumina grains in the mullite–alumina composite prepared from diphasic precursors. © *1998 Chapman & Hall*

1. Introduction

The results of many researchers confirm that α-Al_2O_3 is formed from boehmite-derived gels by a nucleation and growth process [1–4]. Nucleation is the most significant step of this transformation and is mostly concerned with glass-forming gels, which exhibit practically the same crystallization behaviour, including nucleation and crystal growth, as conventionally prepared glasses. In ceramic gels, consideration of nucleation includes the surface, crystal defects and strain energy. In general, the volume of a new phase will not fit perfectly into the space originally occupied by the matrix, and this gives rise to a misfit strain energy. Summing all of these gives the total Gibb's free energy change, ΔG, for the formation of a new phase in a gel [5]

$$\Delta G = -V\Delta G_V - (A_{S_1}\gamma_{S_1g} - A_{S_2g}\gamma_{S_2g}) + A_{S_1S_2}\gamma_{S_1S_2} + V\Delta G_s \quad (1)$$

where G_V is the Gibb's free energy (including the contribution of the crystal defects energy); V is the volume; A is the surface area; γ is the interface energy; γ_{sg} is the solid–gas interface energy; G_S is the misfit strain energy; and S_1 and S_2 are the new and parent phase, respectively.

The driving force for the homogeneous nucleation of a new phase increases if, during the transformation, there is a decrease of the surface (solid–gas interface) and the number of crystal defects. The misfit strain energy term always increases the free energy of the system. That is why the strain energy reduces the effective driving force for homogeneous nucleation.

The strain energy for a nucleus with coherent interface is caused by the lattice misfit between the nucleus and the matrix, and for incoherent interfaces by the volume misfit as a result of the different densities of the newly formed and parent phases. The values of ΔG_S and $\gamma_{S_1S_2}$ (Equation 1) are dependent on the lattice parameters and densities of both phases. If the crystal structures of both phases are very different, it is impossible to form coherent low energy interfaces and then homogeneous nucleation becomes impossible. However, it is often possible to form a coherent nucleus of some other metastable phase [5].

Li and Thomson [6] studied the mullite formation kinetics of a single-phase gel with silicon- and aluminium-containing species mixed at the molecular scale. They used the nucleation and growth model of Avrami; which relates the conversion, X, to time, t, by the following equation

$$X = 1 - \exp(-k_A t^n) \quad (2)$$

where k_A relates to the nucleation and growth rates of the product, and the exponent, n, can have values between 1 and 4, depending on the nucleation and growth mechanisms and the crystal geometry. The rate of nucleation, N', in a condensed system has the following temperature-dependent form

$$N' = A\exp[-(\Delta G_N + \Delta G_D)/kT] \quad (3)$$

where ΔG_N and ΔG_D are the activation energies for nucleus formation and diffusion across the phase boundary, respectively; and A is the pre-exponential constant; k is a constant; and T is the temperature. On

the basis of the results obtained in this study, one of the conclusions is that the rate of mullite formation from single-phase gels is apparently much faster than that in diphasic gels and limited by nucleation mechanisms. The observation of a constant particle size during mullite formation led to the conclusion that single-crystal mullite was formed within each particle, which resulted in equiaxial mullite grains in the sintered microstructure derived from this single-phase gel.

Studies of the transformation kinetics of diphasic aluminosilicate gels [7], show that mullite forms via nucleation and growth of single-crystal mullite grains by a process either interface-controlled or controlled by short-range diffusion.

The objective of present work was to study the structure of a diphasic mullite precursor and the influence of interaction between the alumina and silica components on the alumina phase transitions. The formation of an α-alumina grain in the mullite–alumina composite, especially nucleation and the initial stage of grain growth, was also studied.

2. Experimental procedure

A single alumina precursor was prepared by a precipitation method through addition of an $AlCl_3$ solution into a NH_4OH solution (pH = 8.5). The precipitated suspension was filtered, dispersed into distilled water several times to remove the Cl^- and then dried in air at 100 °C for 10 h. The dried precursor was calcined at 1000, 1200 and 1310 °C for 2 h with a 5 °C min^{-1} heating rate.

A mullite–alumina composite precursor with 10 vol% excess alumina over the stoichiometric mullite composition was also prepared by a coprecipitation method [8]. The washing procedure followed and the subsequent drying were the same as described for the single alumina precursor. The powder was then calcined at 1000 °C for 2 h using a 5 °C min^{-1} heating rate and milled to prepare green bodies by uniaxial pressing at 50 MPa followed by isostatic pressing at 150 MPa. Sintering was carried out at 1400 and 1500 °C for 10 h and 1600 °C for 6 h with a 5 °C min^{-1} heating rate, then polished and thermal etched at temperatures 10% lower than the sintering temperatures for scanning electron microscope (SEM) observation.

The mullite–alumina composite precursor calcined at 1000 °C for 2 h was leached by contact with a 3 wt% HF solution for 10 h and then filtered. The leached precursor was dried at 100 °C and then calcined at 1000 and 1200 °C for 2 h.

The phase transitions and the structural transformations of the powders under different thermal treatment conditions, and of the sintered compacts were identified by X-ray diffraction (XRD, model XDMAX, Rigaku), SEM (model S4100-1, Hitachi) and transmission electron microscopy (TEM, model Hitachi H9000-NA).

3. Results and discussion

The XRD spectra of the single alumina phase precursor after thermal treatment are shown in Fig. 1. The sequence is generally consistent with the results reported in the literature [9]

$$\text{Boehmite} \rightarrow \gamma\text{-}Al_2O_3 \rightarrow \delta\text{-}Al_2O_3 \rightarrow \theta\text{-}Al_2O_3 \rightarrow \alpha\text{-}Al_2O_3$$

but occurs at higher temperatures. The different transition temperatures for the single alumina precursor, observed between this work and similar works reported in the literature namely from γ-(δ- or θ-) Al_2O_3 to α-Al_2O_3, can be attributed to different precursor sources and to the different preparation techniques used [5, 10–12]. Pach *et al.* [5] studied the phase transitions of boehmite-derived alumina gels and detected the α-Al_2O_3 phase at 1040 °C, while Dynys and Halloran [10] formed α-Al_2O_3 at 1150 °C from alum-derived γ-Al_2O_3. The α-Al_2O_3 phase was also formed at 1200 °C from a γ-Al_2O_3 film deposited from a hot-pressed Al_2O_3 target by radio frequency magnetron reactive sputtering deposition in a plasma containing argon and oxygen [11]. In the present

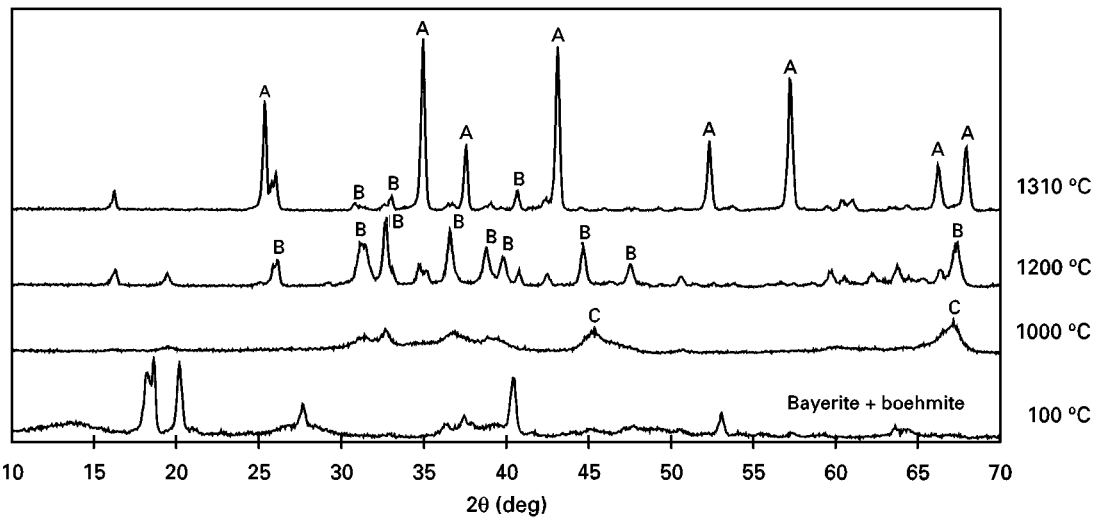

Figure 1 The XRD spectra of the single alumina phases after thermal treatment: (A) α-Al_2O_3, (B) θ-Al_2O_3, (C) γ-Al_2O_3.

work, α-Al_2O_3 was formed at 1310 °C. The relatively higher transition temperatures are probably due to strong agglomeration of the alumina precursor in a lower activated state, which may require high activation energy [13]. Pach *et al.*'s studies [5] also show that isothermal heating time (at 1040 °C) plays a very important role in the process of phase transition from γ-Al_2O_3 to α-Al_2O_3.

Detailed information about phase transitions and structural transformations of the alumina phase in the silica matrix due to thermal treatment has been reported earlier [14]. The results revealed that the transition sequence of the alumina phase when inside the silica matrix is similar to that of single-phase alumina, but occurs at higher temperatures. The alumina reacts with the amorphous silica matrix to form mullite before the phase transition from θ- to α-alumina takes place. In the mullite–alumina composite sintered at 1400 °C, excess alumina still exists in the form of a low crystalline θ-alumina phase, as shown in Fig. 2. This delayed phase transition is attributed to the big difference in crystal structure between α-alumina and crystallized SiO_2. As mentioned above, it is impossible to form coherent low energy interfaces in these conditions. This also makes homogeneous nucleations of both phases impossible. The phase contrast in the SEM micrograph (backscattering signal) in Fig. 3a also shows that there is no α-alumina present in the sintered body. Instead, a metastable mullite phase is formed.

In the mullite–alumina composites, nucleation and grain growth of α-Al_2O_3 takes place at about 1500 °C in the rich alumina regions as revealed by the XRD spectrum shown in Fig. 2. The layered γ-Al_2O_3 texture and the close lattice match between γ- and α-alumina play a vital role in the process of α-alumina nucleation and the initial stage of grain growth. Because there is no compositional change during $\gamma \rightarrow \alpha$ alumina phase transformation, this transformation can only involve

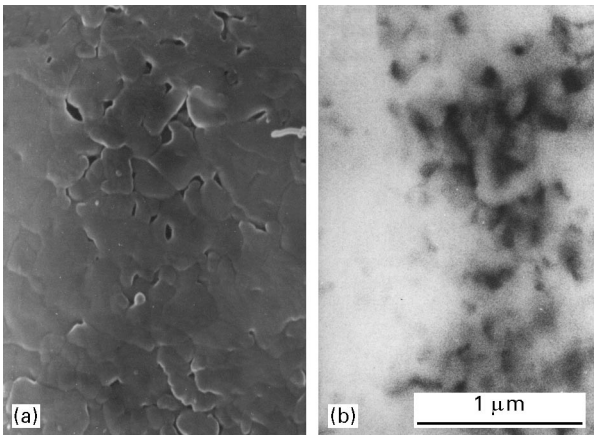

Figure 3 SEM micrograph of the sample sintered at 1400 °C: (a) secondary electron signal, and (b) backscattering electron signal.

short-range transport of Al ions and promote the collective, massive growth of α-alumina grains. The layered γ-alumina texture and the close lattice match between γ- and α-alumina also contribute to the preferred orientations in the crystal growth process [11]. As a result, alumina grains in the sample sintered at 1500 °C appear in the form of platelets, as shown in Fig. 4a. Platelet α-Al_2O_3 grains become well defined after sintering at 1600 °C for 6 h, as shown in Fig. 4b [15].

The XRD spectra of mullite–alumina precursors after leaching and recalcining are shown in Fig. 5. The phase transitions in the process of leaching and recalcining are

Mullite–alumina composite precursor

$$\xrightarrow{\text{HF solution}} AlF_{1.65}(OH)_{1.35} \cdot XH_2O$$

$$\xrightarrow{\text{Recalcination at } 1000\,^\circ\text{C}} \alpha\text{-}Al_2O_3$$

$$\xrightarrow{\text{Recalcination at } 1200\,^\circ\text{C}} \text{well crystallized } \alpha\text{-}Al_2O_3$$

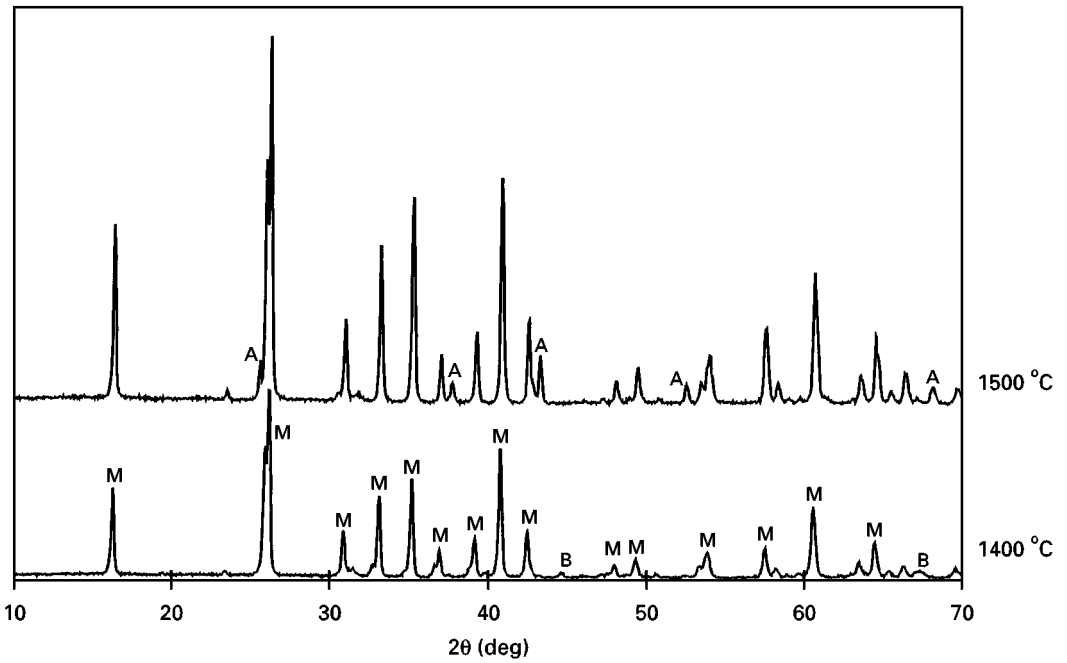

Figure 2 The XRD spectra of the mullite–alumina composite sintered at 1400 and 1500 °C: (A) α-Al_2O_3, (B) θ-Al_2O_3, (M) mullite.

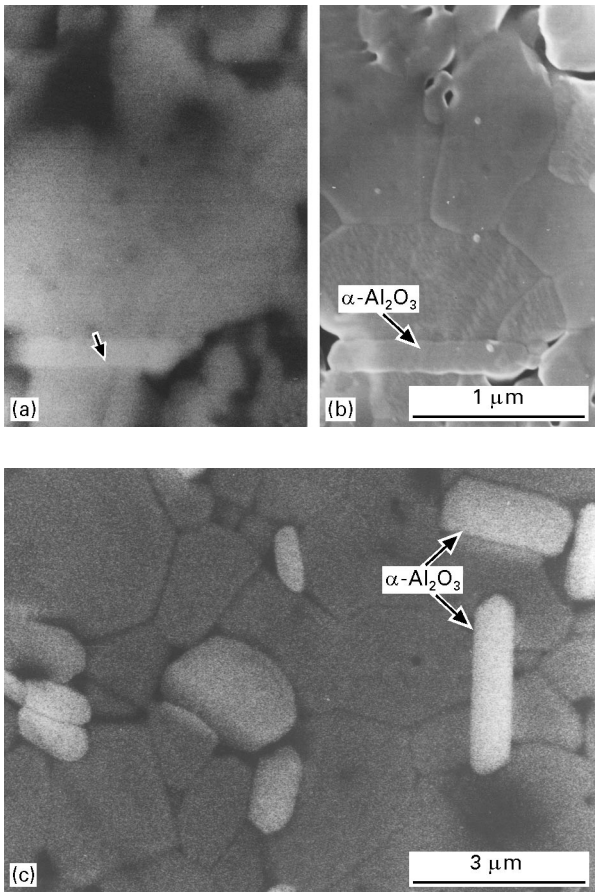

Figure 4 SEM micrograph of the sintered samples: (a) at 1500 °C for 10 h; backscattered; (b) at 1500 °C for 10 h, secondary electron signal; and (c) 1600 °C for 6 h, backscattered.

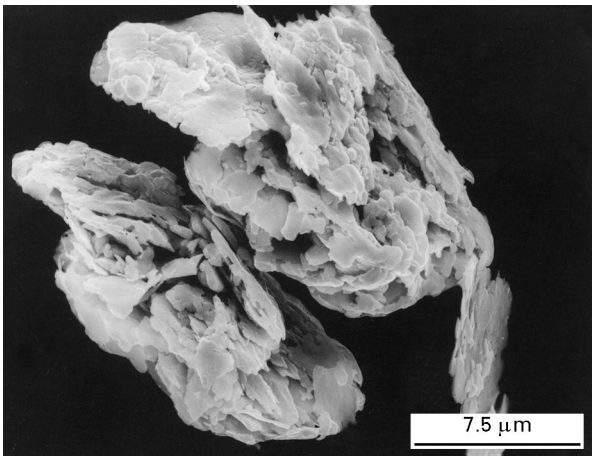

Figure 6 SEM micrograph of the mullite–alumina precursor (calcined at 1000 °C for 2 h).

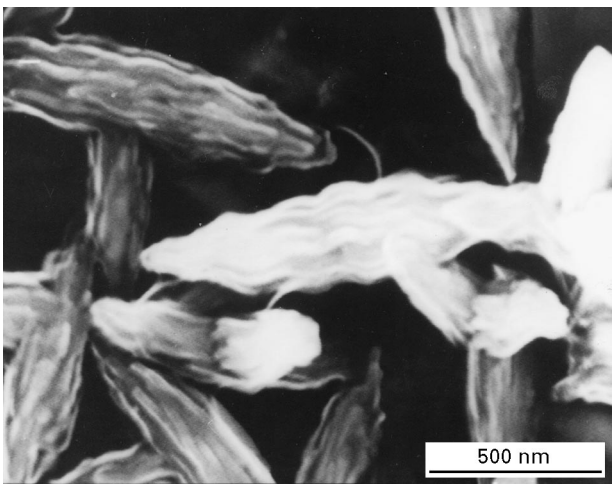

Figure 7 SEM micrograph of the leached mullite–alumina precursor without recalcination.

The SEM micrograph of the mullite–alumina precursor (calcined at 1000 °C) is shown in Fig. 6. It can be seen that the agglomerates are composed of small layered particles. This layered structure is due to the layered γ-Al_2O_3 (or spinel phase) structure. After leaching in dilute HF solution, the agglomerates are broken into nanometre-scale particles in aciculate form as shown in Fig. 7. Compared with the smooth surfaces of the unleached particles there are lots of etch-pit lines in the surfaces of the leached particles that are oriented with the axes of the particles.

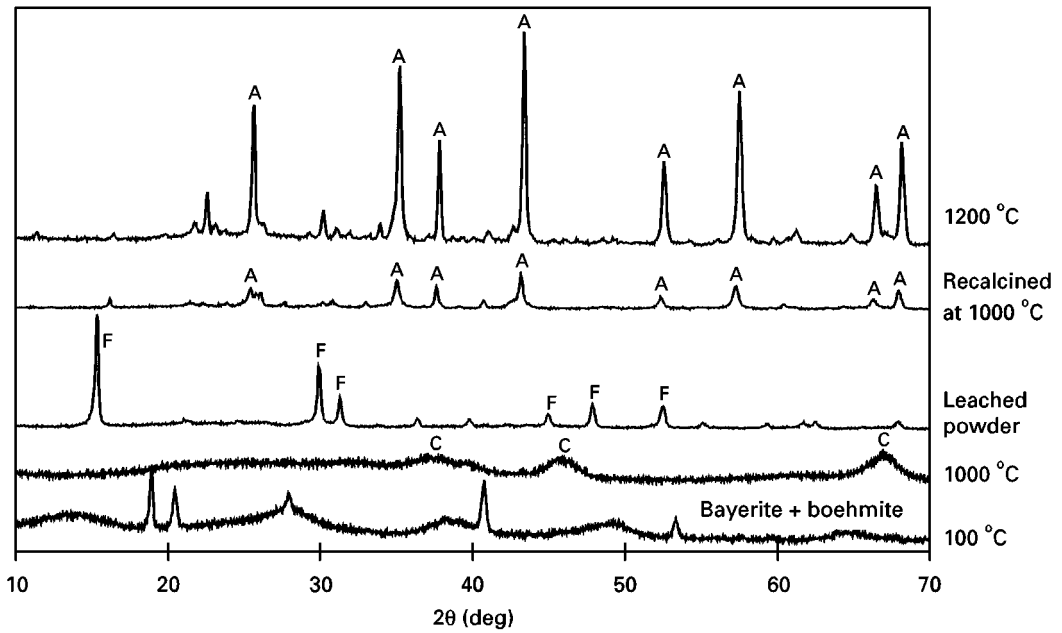

Figure 5 XRD spectra of leached mullite–alumina precursors; after thermal treatment: (A) α-Al_2O_3, (F) $AlF_{1.65}(OH)_{1.35} \cdot XH_2O$, (C) γ-Al_2O_3.

The XRD spectra in Fig. 5 show that α-Al_2O_3 is the dominant phase in the powders recalcinated at 1000 and 1200 °C, indicating that the powder remaining after leaching is mainly composed of alumina components. SEM micrographs of the leached powders recalcined at 1000 °C are shown in Fig. 8a. All the particles are small pieces of transparent platelets that already have been identified as α-alumina. The formation of these thin α-Al_2O_3 platelets could be attributed to the layered structure of the leached powder.

The elongated mullite grains in the pure mullite matrix prepared from this kind of diphasic precursor [8, 16] are likely to be attributed to the structure of the precursor, while a single phase mullite precursor leads to equiaxial mullite grains [16]. With the recalcination temperature increasing to 1200 °C, the degree of crystallization increases as revealed by the XRD spectra shown in Fig. 5. Fig. 8b shows that coalescence of the small thin α-Al_2O_3 platelet has already started.

TEM micrographs (bright field) of the precursor calcined at 1000 °C, unleached and leached, are shown in Fig. 9 (bright field). It seems that the crystallites in the leached powder are well individualized and there is a less amorphous phase existing inside the powder. A TEM micrograph (bright field) of the leached powders recalcined at 1200 °C is shown in Fig. 10; the TEM lattice image indicates that this α-Al_2O_3 platelet is very well crystallized as reflected by the XRD spectrum.

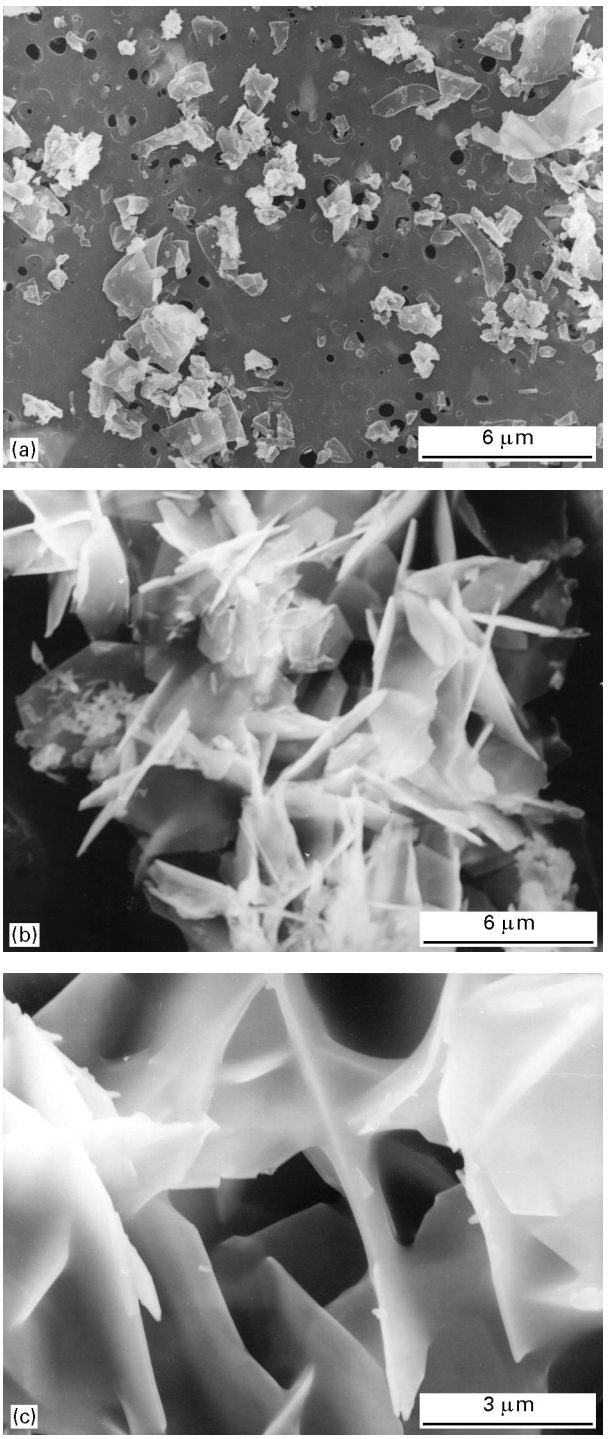

Figure 8 SEM micrographs of leached mullite–alumina precursors after recalcination: (a) at 1000 °C for 2 h, and (b, c) at 1200 °C for 2 h.

4. Conclusions

1. Compared with single alumina phase transitions under thermal treatment, higher temperatures are needed to make alumina phase transitions in diphasic precursors take place. In the mullite-alumina composite no α-Al_2O_3 is formed before mullitization because of the retardation effect exerted by the silica

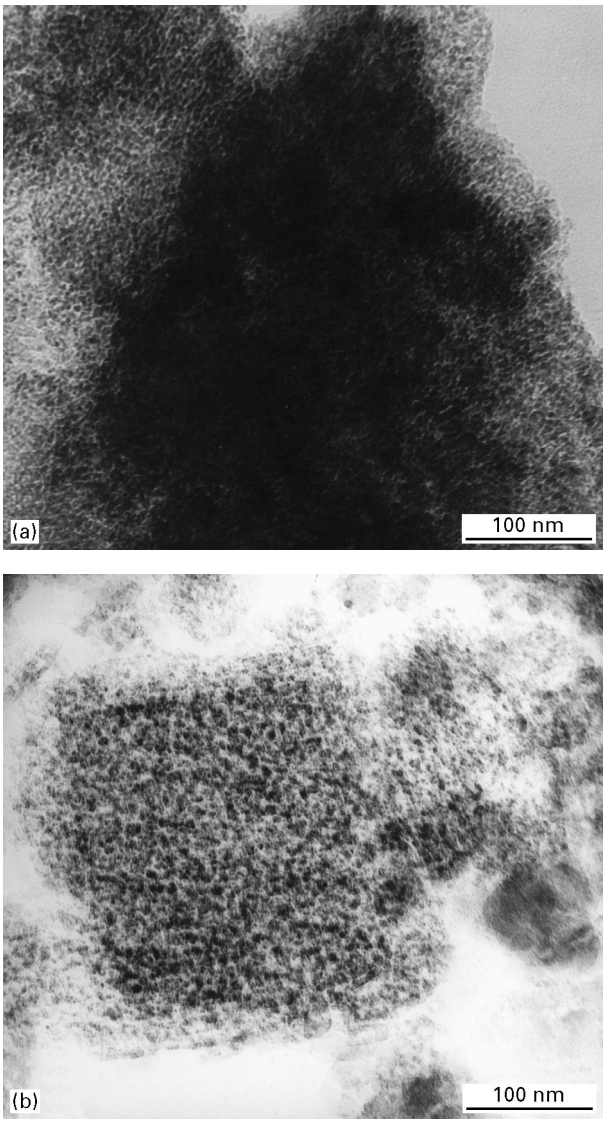

Figure 9 TEM micrographs (bright field) of the precursor calcined at 1000 °C: (a) unleached, and (b) leached.

Figure 10 TEM micrograph (bright field) of the leached precursor after recalcination at 1200 °C.

matrix [17]. As a consequence, an α-alumina phase is formed in the composite matrix at about 1500 °C sintering temperature.

2. By leaching away the silica matrix in the precursor calcined at 1000 °C, the intermediate alumina component remaining was readily transformed into α-alumina after recalcination at the same temperature.

3. The morphology of the leached diphasic precursor and the formation of very fine, thin α-Al_2O_3 platelets after recalcination reveal layered γ-alumina textural characteristics in the diphasic precursor. The formation of α-alumina platelets, specially the nucleation and initial stage of grain growth, in the mullite–alumina composite is likely to be attributed to the lattice match between the layered γ-alumina texture and α-alumina structure.

References

1. G. L. MESSING, M. KUMAGAI, R. A. SHELLEMAN and J. L. McARDLE, in "Science of Ceramic Chemical Processing", edited by L. L. Hench and D. R. Ulrich (Wiley, New York, 1986), Ch. 28, pp. 259–71.
2. F. W. DYNYS and J. W. HALLORAN, *J. Amer. Ceram. Soc.* **65** (1982) 442.
3. *Idem*, in "Ultrastructure Processing of Ceramics, Glasses and Composite", edited by L. L. Hench and D. R. Ulrich (Wiley, New York, 1984), Ch. 11, pp. 142–151.
4. W. YARBROUGH and R. ROY, *J. Mater. Res.* **2** (1987) 494.
5. L. PACH, R. ROY and S. KOMAMENI, *ibid.* **5** (1990) 287.
6. D. X. LI and W. J. THOMSON, *J. Amer. Ceram. Soc.* **73** (1990) 964.
7. WEN-CHENG WEI and J. W. HALLORAN, *ibid.* **71** (1988) 581.
8. MINGHUA ZHOU, J. M. F. FERREIRA, A. T. FONSECA and J. L. BAPTISTA, *ibid.* **79** (1996) 1756.
9. K. WEFERS and G. M. BELL, "Oxides and Hydroxides of Aluminum", Technical Paper No. 19 (Alcoa, Pittsburgh, PA, 1972).
10. F. W. DYNYS and J. W. HALLORAN, *J. Amer. Ceram. Soc.* **65** (1982) 442.
11. TING C. CHOU and TAI G. NIEH, *ibid.* **74** (1991) 2270.
12. MASATO KUMAGAI and G. L. MESSING, *ibid.* **68** (1985) 500.
13. R. K. DWIVEDI and G. GOWDA, *J. Mater. Sci. Lett.* **4** (1985) 331.
14. MINGHUA ZHOU, J. M. F. FERREIRA, A. T. FONSECA and J. L. BAPTISTA, Microstructure Development of Mullite-Alumina Composite from Diphasic Precursor, in Euroceramics IV, Proceedings of the Fourth Euroceramics, Conference, Vol. 1 Part I, edited by C. Galassi and Faenza Editrice (1995) pp. 339–44
15. M. ZHOU, J. M. F. FERREIRA, A. T. FONSECA and J. L. BAPTISTA, *J. Europ. Ceram. Soc.* in press.
16. J. A. PASK, X. W. ZHANG and A. P. TOMSIA, *J. Amer. Ceram. Soc.* **70** (1987) 704.
17. L. PACH, S. KOMARNENI and C. LIU, *J. Porous Mater.* **2** (1995) 131.

Received 31 October 1996
and accepted 5 December 1997